

Rydberg and pulsed field ionization-zero electron kinetic energy spectra of YO

Colan Linton

Physics Department, University of New Brunswick, Fredericton, New Brunswick, E3B 5A3 Canada

Benoit Simard, Hans Peter Loock,^{a)} and Sara Wallin^{b)}

Steacie Institute for Molecular Sciences, National Research Council of Canada, Ottawa, Ontario, K1A 0R6 Canada

Gretchen K. Rothschoepf, Robert F. Gunion,^{c)} Michael D. Morse,^{d)}

and Peter B. Armentrout

Department of Chemistry, University of Utah, Salt Lake City, Utah 84112

(Received 19 April 1999; accepted 24 June 1999)

A spectroscopic study of the Rydberg states of YO accessed from particular rotational levels of the $A^2\Pi_{1/2}$, $v=0$ state has been combined with a pulsed field ionization, zero electron kinetic energy (PFI-ZEKE) investigation. The results provide accurate values of the ionization energy of YO, ionization energy $I.E.(YO)=49\,304.316(31)\text{ cm}^{-1}$ [$6.112\,958(4)\text{ eV}$], and of the rotational constant (and bond length) of the YO^+ cation in its $X^1\Sigma^+$, $v=0$ ground state, $B_0^+=0.4078(3)\text{ cm}^{-1}$ [$r_0=1.7463(6)\text{ \AA}$]. The improved value of $I.E.(YO)$ combined with the known ionization energy of atomic yttrium then leads to the result $D_0^0(Y-O)-D_0^0(Y-O)=0.1041\pm 0.0001\text{ eV}$. Combining this result with the value of $D_0^0(Y^+-O)$ obtained from guided ion beam mass spectrometry yields an improved value of $D_0^0(Y-O)=7.14\pm 0.18\text{ eV}$. The PFI-ZEKE spectra display an interesting channel-coupling effect so that all rotational levels with $J^+\leq J'(A)+0.5$ are observed with high intensity, where J^+ is the angular momentum of the YO^+ cation that is produced and $J'(A)$ is the angular momentum of the $A^2\Pi_{1/2}$ state that is reached when the first photon is absorbed. This is thought to result from the interaction between the dipole moment of the rotating YO^+ core and the Rydberg electron, which can induce changes in l and J^+ subject to the dipolar coupling matrix element selection rule, $\Delta J^+=\pm 1$, $\Delta l=\pm 1$. The channel-coupling mechanism also appears to induce an inverse autoionization process in which an unbound electron with a low value of l is captured either by its low- J^+ YO^+ cation or by a second YO^+ cation with the same value of J^+ . This inverse autoionization process is extremely sensitive to the electron kinetic energy, leading to narrow peaks in the PFI-ZEKE spectrum which are only slightly broader than the laser linewidth employed for this study (0.25 cm^{-1}). © 1999 American Institute of Physics.

[S0021-9606(99)01335-5]

I. INTRODUCTION

An accurately determined ionization energy (I.E.) is very important as an aid towards understanding many of the physical and chemical properties of atoms and molecules. For example, it gives valuable insight into electronic structure and, when used in an appropriate thermodynamic cycle, provides information on bond strengths of the neutral and ionic species. For a diatomic metal-containing molecule, (MX), the bond strengths, D_0 , of the neutral molecule and its cation are directly related to the ionization energies of the metal atom and neutral molecule by

$$D_0(\text{MX}) - D_0(\text{M}^+ - \text{X}) = I.E.(\text{MX}) - I.E.(\text{M}). \quad (1)$$

^{a)}Present address: Department of Chemistry, Queen's University, Kingston, Ontario.

^{b)}Visiting scientist from the Department of Physics, Stockholm University, Box 6730, S-113 85, Stockholm, Sweden.

^{c)}Present address: E. O. Lawrence Berkeley National Laboratory, Mail Stop 2-400, 1 Cyclotron Road, Berkeley, CA 94720.

^{d)}Electronic mail: morse@chemistry.chem.utah.edu

Spectroscopic methods based on the analysis of Rydberg spectra and pulsed field ionization-zero electron kinetic energy (PFI-ZEKE) spectra now allow us to determine the I.E.s of atoms and molecules to high accuracy, and thus gives a precise value for the difference in bond strengths of the neutral molecule and its cation. Thus, accurate I.E. measurements can greatly improve the accuracy of bond strengths which previously had been determined by fairly imprecise thermochemical techniques.

Rydberg and PFI-ZEKE spectra can also provide spectroscopic information on the ground and other low-lying states of cationic species. Such information is greatly needed to rationalize the bonding in transition metal containing cations. Currently, the only cationic transition metal species for which accurate bond lengths are available are V_2^+ ,¹ Ni_2^+ ,^{2,3} VO^+ ,^{4,5} ZrO^+ ,^{6,7} TaO^+ ,⁸ TiF^+ ,⁹ $TiCl^+$,¹⁰⁻¹⁴ YF^+ ,¹⁵ LaF^+ ,^{16,17} VAr^+ ,¹⁸ $CoAr^+$,¹⁹ $CoKr^+$,²⁰ and $ZrAr^+$.²¹

This paper presents the results of investigations on the yttrium monoxide cation (YO^+) carried out jointly at the National Research Council of Canada (NRC) and the Uni-

versity of Utah. At the NRC, two-color Rydberg spectra of YO have been obtained showing Rydberg series converging to the ionization limit for different rotational levels of the $v^+ = 0$ level of the ion. From these series, the ionization energy of neutral YO and the rotational constant of the ground $^1\Sigma^+$ state of YO^+ have been determined. At Utah, two-color PFI-ZEKE spectra have been obtained showing the rotational levels of the ground state of YO^+ as well as Rydberg series converging to these levels. We describe below the combined results of our experiments.

There have been four previous studies dealing with the ionization energy of YO. The first determination is due to Rauh and Ackermann, who used electron impact on an effusive beam of YO to obtain an ionization energy of 5.85 ± 0.15 eV.²² A few months later Liu and Wahlbeck, also using electron impact on an effusive beam of gaseous YO, reported a value of 6.0 ± 0.1 eV.²³ In the same study, Liu and Wahlbeck analyzed the equilibrium reaction $\text{Y}_2\text{O}_{3(a)} \leftrightarrow 2\text{YO}_{(g)} + \text{O}_{(g)}$ over the temperature range 2342–2614 K to derive from a third-law analysis the binding energy, $D_0^0(\text{YO}(g))$, as 7.38 ± 0.09 eV.²³ A few years later, Murad and Hildenbrand, also using electron impact, reported the values of 6.4 ± 0.5 eV and 6.0 ± 0.3 eV for the I.E. of YO^+ .²⁴ More recently, Sievers *et al.* investigated the reaction of Y^+ with CO and the collision-induced dissociation of YO^+ with Xe as a function of the kinetic energy using guided ion beam mass spectrometry to derive the binding energy of YO^+ , $D_0^0(\text{Y}^+ - \text{O})$, as 7.24 ± 0.18 eV.²⁵ This value was used in the thermodynamic cycle shown in Eq. (1) along with I.E.(Y) and $D_0^0(\text{YO})$ to derive a value of 6.39 ± 0.22 eV for I.E.(YO). From this review, it is clear that the ionization energy of YO is not particularly well established. Considering the importance of YO in high-temperature chemistry, a more accurate value is needed.

There have been several measurements of the dissociation energy of YO, the most recent being the work by Liu and Wahlbeck mentioned above.²³ All of these experimental studies were carefully and critically assessed by Pedley and Marshall, who recommended a value of 7.41 ± 0.12 eV for $D_0^0(\text{YO})$.²⁶ The only determination of $D_0^0(\text{Y}^+ - \text{O})$ has been from the work of Sievers *et al.* mentioned above, which provided a value of $D_0^0(\text{Y}^+ - \text{O}) = 7.24 \pm 0.18$ eV.²⁵

Besides the obvious need for better accuracies in the energetics of YO and YO^+ , this work provides an opportunity to test and calibrate the newly built PFI-ZEKE spectrometer at the University of Utah. The observation of long Rydberg progressions yields very accurate ionization limits that provide calibration standards for the observed PFI-ZEKE features.

II. EXPERIMENTAL DETAILS

The experimental setup at the NRC has been described previously.²⁷ This section will therefore focus on modifications that have been made and details that are of relevance in this set of experiments. The molecules under study were prepared in a laser ablation source housing a rotating yttrium rod that was vaporized using a mildly focused 355 nm, 5 mJ/pulse Nd:YAG laser beam. Through this plasma

streamed a pulsed jet²⁸ of a mix of $\sim 1\%$ oxygen in 5000 Torr of helium. The gas expanded supersonically into high vacuum (approx. 10^{-6} Torr) and the jet was skimmed approximately 200 mm downstream by a faceplate with a 5 mm pinhole. The resulting molecular beam entered the first stage of a Wiley–McLaren time-of-flight mass spectrometer (TOF-MS).²⁹ Using separate high-voltage power supplies for the repeller grid, the extraction grid (both typically at 2000 V), and the pulsed extraction voltage (typically 500–700 V subtracted from the extraction grid voltage), it was possible to not only space-focus the ions but also to adjust the residual field that was present prior to the extraction pulse. The resolution ($m/\Delta m$) of the TOF-MS was about 300, far more than necessary to separate YO^+ from any other masses which might be present.

The Utah experiments were conducted using a similar instrument. An yttrium metal disk (Alfa) was rotated and translated while being held against a stainless-steel block, through which a hole had been drilled to admit a beam of focused 248 nm KrF excimer radiation (10 mJ/pulse) which ablated the metal. A magnetically actuated double solenoid valve³⁰ was employed to pulse a flow of helium through a 2 mm channel drilled just under the surface of the stainless-steel block, thereby entraining the ablated atomic and molecular species. These were carried approximately 3 cm before undergoing supersonic expansion through a diverging nozzle into a low-pressure region ($\sim 10^{-4}$ Torr, maintained by a Varian VHS 10 diffusion pump). Although high-purity helium (99.99%) was used as the carrier gas with a backing pressure of ~ 125 psi, sufficient oxygen was present to form large quantities of YO.

The molecular beam was roughly collimated by a 5 mm conical skimmer as it entered the spectroscopy chamber. A pair of deflection plates about 5 cm in length, 3 cm wide, and about 2 cm apart, was located immediately following the skimmer. These were used to provide a static electric field ranging from 10–50 V/cm which served to deflect most of the ions and electrons produced during laser ablation. Neutral molecules then entered a spectroscopy region which was evacuated by a turbomolecular pump ($\sim 10^{-6}$ Torr, Varian, Turbo V1000). This second chamber was constructed to function either as a resonant two-photon ionization (R2PI) spectrometer with mass-specific detection or as a pulsed field ionization-zero electron kinetic energy (PFI-ZEKE) spectrometer with electron detection. To change from one mode of operation to the other required only a change in the voltages applied to the electrodes, along with a change of detector.

As in the NRC instrument, for ion detection the Utah instrument employed a Wiley–McLaren design consisting of a repeller, draw-out grid, and ground grid as shown in the inset of Fig. 1.²⁹ A metal mesh was attached to all three electrodes using the method of Weisshaar³¹ to stretch the mesh taut and thereby establish more uniform electric fields. Static voltages of 768 and 920 V, respectively, were applied to the draw-out grid and repeller, for R2PI scans of YO. As the ions left the acceleration region, they passed through deflectors which were used to overcome the molecular beam velocity and direct the ions to the detector. Ions were de-

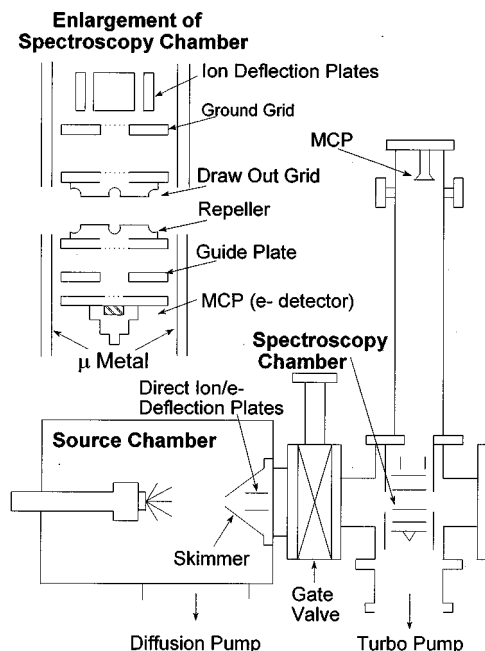


FIG. 1. Schematic diagram of the Utah PFI-ZEKE instrument, illustrating details of the ionization region in the inset.

ected 127 cm up the flight tube by a dual microchannel plate detector (Galileo, 3025) equipped with a custom-built 50 Ω anode assembly.^{32,33}

The PFI-ZEKE experiments were accomplished by detecting the electron signal at a second dual microchannel plate detector (Hamamatsu, F2221-21) with another custom-built 50 Ω anode assembly, located about 4.7 cm below the interaction region. During a PFI-ZEKE experiment, the draw-out and repeller grids were both held at a potential of -18.0 V for a period of 3 μs after the spectroscopy lasers were fired. This delay allowed the radio frequency noise associated with firing the excimer lasers to decay, and also allowed any directly ejected electrons to disperse under the combined influence of their initial kinetic energy and the stray electric field which was inevitably present. In all of the spectra reported in this paper, the draw-out grid was then pulsed to a voltage ranging from -19 to -19.5 V. The high Rydberg levels populated by the lasers thus evolve in a nominal electric field of 0 V/cm for 3 μs , at which time the field is pulsed to a value between 0.28 and 0.42 V/cm to eject the Rydberg electrons. Two layers of μ -metal magnetic shielding were also placed around the spectroscopy region, with holes cut at appropriate places to allow the molecular and laser beams to enter and exit.

Spectroscopic information was obtained from a two-color pump and probe scheme using two tunable pulsed dye lasers pumped by either Nd:YAG or excimer lasers. The first (pump) laser was used to excite the molecule, which was then ionized using the second harmonic radiation of a second tunable dye laser. The excitation and ionization procedures were the same in both the NRC and Utah experiments, the only difference being in the method of detection. As a preliminary step, R2PI experiments were performed in which the excitation laser was scanned in the 16 300 cm^{-1} region

while the ionization laser was held at a fixed frequency capable of ionizing the electronically excited states. These served to identify the initial $A^2\Pi_{1/2}-X^2\Sigma^+$ transitions. The Rydberg (at NRC) and PFI-ZEKE (Utah) experiments were performed by tuning the excitation radiation successively to individual rotational lines in the R_1 branch of the 0-0 band so that, in each case, the YO molecule was excited to a particular rovibrational state. The Rydberg and PFI-ZEKE spectra were then obtained by scanning the ionization laser through the 32 900–33 000 cm^{-1} region [16 450–16 500 cm^{-1} , frequency doubled with a potassium dihydrogen phosphate (KDP) crystal] near the ionization energy and monitoring the signal resulting from pulsing the ionization field as a function of ionization laser frequency. In the Rydberg experiments, the *photoion* signal was detected using three stacked microchannel plates, amplified 125-fold and recorded and processed using a 286/16 MHz PC. In the PFI-ZEKE experiments, the *electron* signals were amplified, digitized, and collected by a 386-based personal computer. The data were then summed and stored for subsequent analysis. The computer also controlled the timing of the nozzle and laser pulses and directed the scanning of the dye lasers. Operationally, it was found that to avoid stray electrons it was necessary to fire the spectroscopy lasers approximately 10–15 μs earlier in time when performing PFI-ZEKE experiments as compared to the optimal timing for R2PI experiments. This was required to reduce the background electron signal which was present when probing in the most intense part of the metal cluster pulse.

In the present experiments, the $v=0$ level of the $A^2\Pi_{1/2}$ state of YO was excited using rhodamine 610 laser radiation. The pulsed pump and probe lasers at the NRC were calibrated using both a wavemeter (Candela) and the tabulated lines of a Fe–Ne hollow cathode lamp.³⁴ At Utah, the spectra were calibrated by the simultaneous collection of an I_2 absorption spectrum which was subsequently compared to the I_2 atlas of Gerstenkorn and Luc.^{35,36} The excitation frequency was calibrated directly, while the ionization frequency was calibrated using the fundamental frequency of the dye laser rather than the frequency-doubled radiation.

III. RESULTS AND ANALYSIS

A. Analysis of Rydberg series

In the NRC experiments, the pump laser was set to excite each rotational transition in the R_1 branch from $R_1(3)$ to $R_1(11)$ and, for each of these transitions, the probe laser was scanned to the ionization threshold. A portion of the spectrum obtained with the pump exciting the $R_1(6)$ transition is shown in Fig. 2. A large number of lines, which are shown to form a Rydberg series, are clearly seen in the spectrum. All the spectra, from each of the nine rotational levels excited, showed similar features and, in each case, a Rydberg series was observed, converging to a different rotational level in the cation. Rydberg series were also observed in four of the Utah PFI-ZEKE spectra as described below (Sec. III B).

The term values of the Rydberg levels were determined by adding the term value of the excited $A^2\Pi_{1/2}$ level, calculated from the spectroscopic constants,³⁷ to the wave number

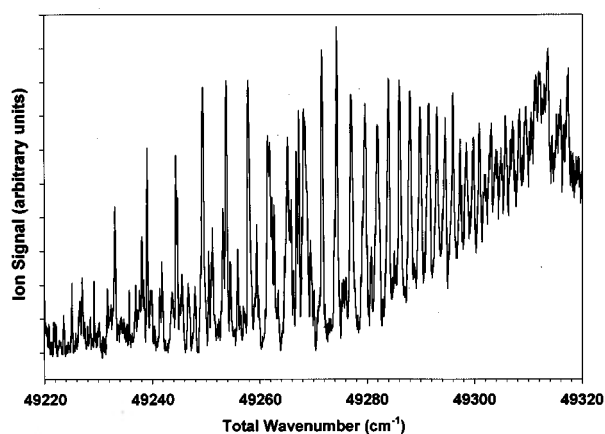


FIG. 2. An example of the Rydberg spectra collected for YO. In this scan, the first tunable laser was set to the $R_1(6)$ excitation of the $A^2\Pi_{1/2}$, $v' = 0 \leftarrow X^2\Sigma^+$, $v'' = 0$ band, thereby populating the $J'(A) = 7.5e$ level of the $A^2\Pi_{1/2}$, $v' = 0$ state. The second laser was then scanned near the ionization threshold, and high Rydberg states were exposed by pulsed field ionization and time-of-flight mass spectrometric detection of the resulting YO^+ cations. The strongest lines correspond to Rydberg states converging to $J^+ = 8$, while many of the weaker lines correspond to Rydberg states converging to $J^+ = 6$. Although other weak lines are present, they cannot be readily identified as Rydberg states converging to a particular rotational level of the cation.

of the probe laser. The analysis then proceeded as follows:

(1) At each J , the term values were fitted to the Rydberg expression

$$T_n(J) = T^+(J^+) - R/n^{*2}, \quad (2)$$

where $T^+(J^+)$ is the ionization energy of the J^+ level of the cation, R is the Rydberg constant for YO, $109\,736.74\text{ cm}^{-1}$, and n^* is the effective principal quantum number of the Rydberg level, given by $n^* = (n - \mu)$ where μ is the quantum defect. The fits gave values of the ionization energies and n^* at each J . For the NRC data, the values of n^* for the fitted lines varied from ~ 30.1 to ~ 62.1 where the fractional part of n^* was always around 0.1 (i.e., the quantum defect was ~ 0.9) and varied randomly between 0.068 and 0.131 (i.e., $\mu = 0.932\text{--}0.869$). For the Utah data, Rydberg series were fitted for initial excitations of $R_1(4)$ to $R_1(7)$, and n^* for the fitted lines was found to be in the range $\sim 53.1\text{--}98.1$ and the fluctuations in the fractional part were greater than those in the NRC data. There was some overlap in the data from the two experiments from $R_1(6)$ and $R_1(7)$ excitation, and this enabled us to check the relative calibration of the lasers in the two experiments. The ionization energies from the two experiments agreed well, to within 0.03 cm^{-1} , which is excellent considering the different ranges of n^* covered by the experiments and the considerably longer extrapolation required when fitting the NRC data.

(2) For the $R_1(4)\text{--}R_1(7)$ data, the results of the Utah and NRC experiments were fitted together covering the range $n^* = 30.1\text{--}98.1$ to give slightly revised values of the ionization energies and n^* . Because variations in the quantum defect, mentioned above, showed no systematic trend with J , they were averaged and the mean value of $\mu = 0.903(20)$ was obtained. The Rydberg series were then

TABLE I. Rydberg series limits for various rotational levels of YO^+ .

J^+	Series limit (cm^{-1}) ^a (combined Rydberg data)	Series limit (cm^{-1}) ^b (Utah ZEKE data)	Difference (cm^{-1})
0		49 303.47	
1		49 304.31(8)	
2		49 306.21(6)	
3		49 308.63(11)	
4		49 311.93(17)	
5	49 316.55	49 315.93(24)	0.62
6	49 321.48	49 320.95(21)	0.53
7	49 327.18	49 326.48(22)	0.70
8	49 333.68	49 332.90(25)	0.78
9	49 341.01	49 340.18(17)	0.83
10	49 349.11	49 348.14(47)	0.97
11	49 358.11	49 357.64(14)	0.47
12	49 367.93	49 366.69	1.24
13	49 378.61		

^aFitted parameters: I.E. ($J^+ = 0$) = $49\,304.316(31)\text{ cm}^{-1}$, $B = 0.4078(3)\text{ cm}^{-1}$. These are the preferred values.

^bFitted parameters: I.E. ($J^+ = 0$) = $49\,303.728(58)\text{ cm}^{-1}$, $B = 0.4054(8)\text{ cm}^{-1}$. Values in parentheses in the table are the 1σ error limits obtained by comparing line positions measured from different scans, in units of 0.01 cm^{-1} .

all refitted keeping μ fixed at this value; the ionization energies obtained are listed in Table I. These ionization energies represent the rotational levels of the cation and were then used to determine the true ionization energy as described below. Figure 3 shows a Rydberg plot of the data at all J s. The plots are clearly linear and illustrate how well the data from the two experiments blend together.

(3) Although, for each transition, the J values of the ground and excited state of the pump transition were known, the value of the rotational quantum number of the cation, J^+ , to which the Rydberg series converged, was not known. To determine this and the true ionization energy and B value for the cation, the rotational term values of the cation were fitted to the usual expression, $T^+(J^+) = T^+(0) + B^+J^+(J^+ + 1)$, where $T^+(0)$ is the true, $J = 0$, ionization energy and B^+ is the rotational constant of the ground $^1\Sigma^+$ state of the cation.

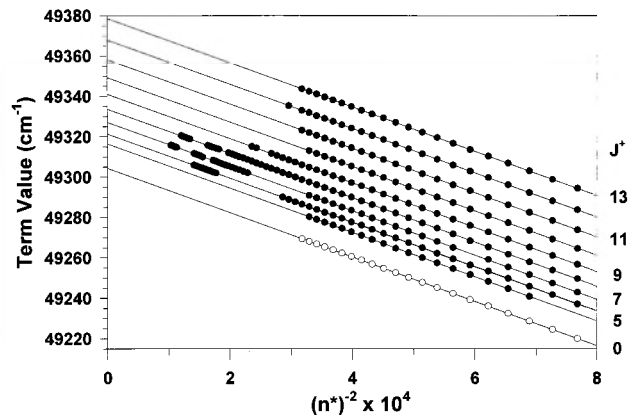


FIG. 3. Rydberg plot of the measured term values as a function of $(n - \delta)^{-2}$, or $(n^*)^{-2}$. For each value of J^+ these data points should fit onto a line of slope $-R$, as is evident from the figure. The isolated data points toward low values of $(n^*)^{-2}$ are taken from the data collected at the University of Utah, as displayed in Fig. 5.

TABLE II. Term values and rotational constants for the $J=0$ levels of Rydberg states of YO.

n^*	T_n (cm^{-1})	B (cm^{-1})
31.097	49 190.35	0.4101
32.097	49 197.73	0.4079
33.097	49 204.15	0.4078
34.097	49 209.80	0.4083
35.097	49 215.32	0.4072
36.097	49 220.07	0.4081
37.097	49 224.59	0.4079
38.097	49 228.72	0.4080
39.097	49 232.55	0.4080
40.097	49 236.21	0.4072
41.097	49 239.32	0.4080
42.097	49 242.40	0.4079
43.097	49 245.24	0.4078
44.097	49 247.91	0.4078
45.097	49 250.32	0.4083
46.097	49 252.64	0.4083
47.097	49 254.79	0.4088
48.097	49 256.88	0.4081
49.097	49 258.95	0.4069
50.097	49 260.65	0.4078
51.097	49 262.34	0.4074
52.097	49 263.93	0.4073
53.097	49 265.39	0.4077
54.097	49 266.80	0.4077
55.097	49 268.09	0.4084
56.097	49 269.33	0.4080

The fit enabled us to determine J^+ for each Rydberg series limit and showed that $J^+ = J(A^2\Pi_{1/2}) + 1/2$. After fixing J^+ and refitting the data, the final values obtained were $T^+(0) = 49\,304.316(31)\text{ cm}^{-1}$ and $B^+ = 0.4078(3)\text{ cm}^{-1}$.

(4) The above method has allowed us to assign the rotational levels, determine the rotational constant of the cation, and calculate the I.E. at $J=0$. However, it did not tell us the rotational quantum number of the excited Rydberg levels. To determine this, a rotational fit was done in order to find the value of J and also $T_n(0)$ and B_n for each individual Rydberg state between $n^* = 32.097$ and 56.097 . It was found that the rotational quantum number was an integer, equal to J^+ in the cation. This is as expected, as the Rydberg electrons are far away from the nucleus and the states are described by Hund's case (*d*) in which the rotational quantum number, R , determines the rotational energy as given by $T_n(R) = T_n(0) + B_n R(R+1)$. The results also show that the B value does not change with n and is equal to that of the ion. The T_n values give a Rydberg series of rotationless levels which converges to the true ionization energy, $T^+(0)$. The term values and B values of all the observed Rydberg states are listed in Table II and the rotational plots for all the Rydberg states are shown in Fig. 4. The B values of all 25 Rydberg levels were averaged and the $T_n(0)$ values were fitted to the Rydberg expression to give $T^+(0) = 49\,304.329(24)\text{ cm}^{-1}$, $\mu = 0.909(67)$, and $B = 0.40796(61)\text{ cm}^{-1}$. These are based only on results of the NRC experiments, as there was insufficient rotational information to enable us to perform these fits on the Utah data. For this reason, the results of the previous fit, i.e., $T^+(0) = 49\,304.316(31)\text{ cm}^{-1}$, $\mu = 0.903(20)$, and $B^+ = 0.4078(3)\text{ cm}^{-1}$ are taken as the final values.

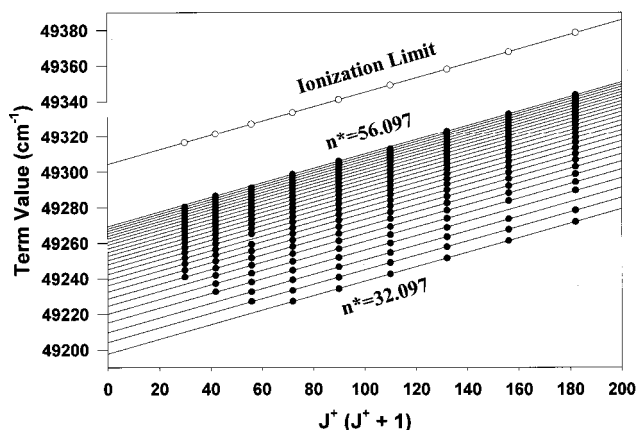


FIG. 4. Rotational plot of the measured term values as a function of $J^+(J^++1)$. Data points corresponding to the same Rydberg state should fall on a straight line with slope B . It is evident that these data conform precisely to this expectation.

B. Results of PFI-ZEKE experiments

PFI-ZEKE spectra were collected by tuning the excitation laser to the $R_1(2) - R_1(7)$ lines of the $A^2\Pi_{1/2} - X^2\Sigma^+ 0-0$ band, then scanning the second laser across the region of the ionization threshold while collecting the signal due to zero kinetic energy (ZEKE) electrons. The spectra obtained via this method are displayed in Fig. 5, shifted in energy so that the abscissa provides the total energy of the system above the $v=0, N=0, J=1/2$ level of the $X^2\Sigma^+$ ground state. For all spectra except the scan using the $R_1(6)$ line, the pulsed ionization field was set to 0.28 V/cm . When the scan employing the $R_1(6)$ line was collected, the weaker overall signal obtained that day required a higher pulsed ionization

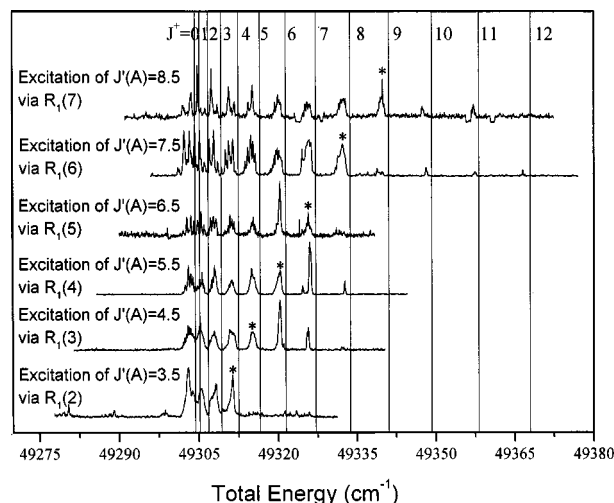


FIG. 5. PFI-ZEKE spectra obtained via initial excitation of $R_1(2) - R_1(7)$, followed by pulsed field ionization using a 0.28 V/cm field [0.42 V/cm for the $R_1(6)$ excitation] and detection of the electron signal, as discussed in the text. The vertical lines give the total wave numbers of the convergence limits of the Rydberg series, and generally lie 0.3 to 1.3 cm^{-1} to the blue of the observed PFI-ZEKE peaks. This is presumably due to a residual field of $2 - 45\text{ mV/cm}$ in the Utah PFI-ZEKE spectrometer, and is a nearly unavoidable problem in PFI-ZEKE work. The dominant Rydberg series for each excitation corresponds to $J^+ = J'(A) + 0.5$, and this convergence limit is indicated in each spectrum by an asterisk.

field of 0.42 V/cm. Assuming that the pulsed field ionization of the Rydberg electron follows a diabatic process, levels lying within roughly $4\sqrt{\mathcal{E}}\text{ cm}^{-1}$, where \mathcal{E} is the field strength in V/cm, will be field ionized.^{38,39} This implies that Rydberg levels lying within 2.1 cm^{-1} [2.6 cm^{-1} for the $R_1(6)$ scan] will be field ionized. These calculated values are roughly in agreement with the widths of the broader features observed in the spectra.

The broader features in Fig. 5 correspond to specific ionization limits of YO, with the Rydberg states that converge to these limits being field ionized if they lie within the ionizable range. Thus, the high-energy edge of these broad features represents the best estimate of the energies of the rotational states of YO^+ which can be obtained from the PFI-ZEKE process. Somewhat disturbingly, the location of these edges varies somewhat from scan to scan, making precise measurements difficult or impossible. The average values of the various ionization limits measured in this way from the spectra displayed in Fig. 5 are listed in Table I along with the standard deviation obtained by comparing values measured in different scans. Table I demonstrates that the ionization limits determined in this way are uniformly lower than those determined by the extrapolation of the Rydberg series. A likely cause of this discrepancy, and of the variation in these measurements from scan to scan, is the probable existence of small, uncontrolled, residual electric fields in the Utah spectrometer. These lead to the destruction of the highest Rydberg states by field ionization prior to the application of the pulsed field, thereby shifting the high-energy edge of the observed features to lower energies. Employing the usual formula for the shift of the ionization energy due to a static electric field,^{38,39}

$$\Delta E(\text{cm}^{-1}) = 6.12\sqrt{\mathcal{E}(\text{V/cm})}, \quad (3)$$

we find that the shifts observed in our experiments ($0.27\text{--}1.30\text{ cm}^{-1}$) are explained by the existence of uncontrolled residual fields in the range of $2\text{--}45\text{ mV/cm}$. It is easy to imagine that stray fields of this magnitude could be present. They could originate from the electrodes and walls of the chamber, but it is more likely that they arise from ions within the molecular beam itself. These ions could be produced in either the original laser ablation plasma or from the multiphoton ionization of other species in the molecular beam. In either case, it is difficult to reduce their concentration sufficiently to eliminate this problem. Whatever their cause may be, these varying shifts in the PFI-ZEKE ionization limits make the PFI-ZEKE method less reliable than the analysis of the Rydberg data. It should be realized, however, that these shifts introduce an error of only $1 \times 10^{-4}\text{ eV}$, such that only the most precise work will be affected.

As is apparent in Fig. 5, superimposed on these broader features is a sort of fine structure in which the lines become more widely spaced as one moves toward lower frequencies. This is especially evident in the spectra obtained via the $R_1(7)$ and $R_1(6)$ transitions, although it is also observed in the spectra obtained via $R_1(5)$ and $R_1(4)$. These features are similar to the spectra recorded at the NRC, and are, in fact, the extension to higher wave numbers of the Rydberg series

observed there. The wave numbers of these closely spaced, discrete transitions were measured, combined with the NRC data set, and analyzed as described above.

IV. DISCUSSION

A. The nature of the observed Rydberg progression

For the main Rydberg series, the rotational quantum number, J^+ , of the $X^1\Sigma^+$ state of the cation is given by $J^+ = J(A^2\Pi_{1/2}) + 0.5$, i.e., $\Delta J = 0.5$. The R_1 pump transition involves e parity levels in both states and the rotational levels of the $1\Sigma^+$ state of the cation are all of e parity. Therefore, the ionization transition, $\text{YO}(A^2\Pi_{1/2}) \rightarrow \text{YO}^+(1\Sigma^+)$, is $e \rightarrow e$. A recent amendment by Watson⁴⁰ to the parity selection rules of Xie and Zare⁴¹ shows that, for an $e \rightarrow e$ transition, $\Delta J - 0.5(-1)^n + l = \text{odd}$, where n is the number of electrons and l is the orbital angular momentum quantum number of the photoelectron (in this case, the Rydberg electron). As YO has an odd number of electrons, and $\Delta J = 0.5$ in the present case, this gives $0.5 + 0.5 + l = \text{odd}$ so that l for the Rydberg electron is even.

It was initially quite puzzling to us that the only rotational lines evident in the Rydberg spectra are those which carry the $2\Pi_{1/2}J'e$ level to a state of the ion core with $J^+ = J'(A) + 0.5$. However, upon closer inspection, a series of somewhat weaker Rydberg transitions corresponding to $J^+ = J'(A) - 1.5$ is also present. This is also consistent with an even value of l . Other Rydberg series are also present, but these are reduced in intensity as compared to the main series. Furthermore, these weaker lines appear to correspond to different Rydberg series and not to other branches of the primary Rydberg series. As far as we can discern, the primary Rydberg series observed here displays only two identifiable branches, corresponding to $J^+ = J'(A) + 0.5$ and $J^+ = J'(A) - 1.5$.

In general, transitions between Hund's case (*a*) states and Hund's case (*d*) Rydberg states are complex, with a large number of branches.⁴² The number of branches expected increases as the value of l is increased, so the observation of only two branches in the present study suggests that l is small. In fact, the observed spectra are entirely consistent with a dominant Rydberg progression consisting of an ns Rydberg electron coupled to a $1\Sigma^+$ ion core. The resulting $2\Sigma^+(d)$ state is similar to a $2\Sigma^+(b)$ state, in which the spin angular momentum of the unpaired σ electron is uncoupled from the internuclear axis, leading to a situation in which the angular momentum excluding electron spin, N , defines the rotational levels according to $E_{\text{rot}}(N) = BN(N+1)$, and a spin splitting then results from the coupling of $S = 1/2$ to N to give $J = N \pm 1/2$. In the Hund's case (*d*) $2\Sigma^+$ state, the rotational levels are defined by the quantum number of the underlying YO^+ cation, J^+ , which is analogous to N in the $2\Sigma^+(b)$ case, and are expected to follow the usual energy formula, $E_{\text{rot}}(J^+) = BJ^+(J^+ + 1)$. The coupling of the ns Rydberg electron to J^+ then leads to levels with $J = J^+ \pm 0.5$. The splitting between these levels is expected to be unmeasurable in our experiment, as it decreases proportionally to $(n^*)^{-3}$.⁴³ For transitions from the e levels of a $2\Pi_{1/2}$ state, the only branches which may be observed are the P_1 ,

Q_{21} , and R_1 branches, which terminate on levels with $J^+ = J'(A) - 1.5$, $J'(A) + 0.5$, and $J'(A) + 0.5$, respectively. These are precisely the transitions observed in our spectra, which display greater intensity in the $J^+ = J'(A) + 0.5$ branch, as is expected from a detailed consideration of the line strengths.⁴³

The alternative assignment for the dominant Rydberg progression is that it corresponds to an nd Rydberg progression. If this were the case, branches corresponding to $J^+ = J'(A) - 3.5$, $J'(A) - 1.5$, $J'(A) + 0.5$, and $J'(A) + 2.5$ might be expected, although the intensities of the outer branches could be quite weak, depending on the atomic character of the 6π electron in the $^2\Pi_{1/2}$ intermediate state.⁴³ At this point in time, all that can be said with certainty is that the dominant Rydberg progression is consistent with either an ns or an nd Rydberg series. Nevertheless, the observation that l is even indicates that the 6π electron is primarily $5p\pi$ in character, since a $4d\pi$ electron would tend to give transitions to Rydberg levels with odd values of l .⁴³

B. Electronic-rotational coupling in the PFI-ZEKE process

Given that the dominant Rydberg series observed corresponds to $J^+ = J'(A) + 0.5$, one might expect a single rotational level to dominate each of the PFI-ZEKE spectra displayed in Fig. 5. The identification of weaker transitions to Rydberg levels with $J^+ = J'(A) - 1.5$, some of which are observed in Fig. 2, would lead one to expect the state with $J^+ = J'(A) - 1.5$ also to be observed in the PFI-ZEKE spectra, but at reduced intensity. The existence of so many additional rotational features in the spectra displayed in Fig. 5 demonstrates that either a mechanism exists for converting energy between rotational and electronic degrees of freedom in the Rydberg states of YO, or that additional Rydberg progressions gain significant oscillator strength at energies within 100 cm^{-1} of the ionization limit, where they are difficult to resolve. This latter possibility seems unlikely, unless the oscillator strength is transferred to the other Rydberg progressions through some sort of mixing process.

It is noteworthy that each of the PFI-ZEKE spectra shows a series of strong features that correspond to values of J^+ ranging from small values up to $J^+ = J'(A) + 0.5$. Additional rotational levels are observed beyond $J^+ = J'(A) + 0.5$; however, these have significantly reduced intensity except in the spectra collected from $J'(A) = 4.5$ and 5.5 [$R_1(3)$ and $R_1(4)$ excitation]. This suggests that the main source of intensity in the PFI-ZEKE spectra is the same $J^+ = J'(A) + 0.5$ Rydberg states that are observed to be intense in the lower energy range. However, unlike the Rydberg spectra displayed in Fig. 2, the PFI-ZEKE spectra exhibit features corresponding to $J^+ = J'(A) - 1.5$, which are quite similar in intensity to those corresponding to $J^+ = J'(A) + 0.5$. In addition, features corresponding to *odd* values of $J'(A) - J^+ + 0.5$ are also observed. Features of this type, which would require odd values of l for the Rydberg electron, are not evident and assignable in the Rydberg spectra collected either in Utah or in Ottawa. While they may be present in the spectra, their intensity must be substantially less than that of the dominant Rydberg progression, and they

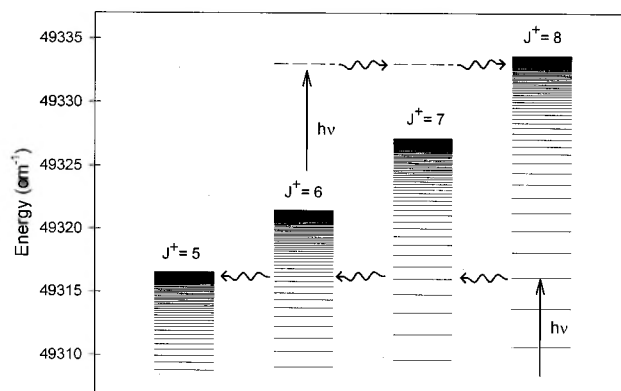


FIG. 6. Channel-coupling interactions in the high Rydberg and continuum states of YO. Excitation to a Rydberg state in the $J^+ = 8$ manifold lying near $49\,316\text{ cm}^{-1}$ prepares a state with $n^* \sim 79$, but dipolar coupling can increase l and decrease J^+ leading to a mixed Rydberg state with significant $J^+ = 5$ character. This coupling process is indicated by the arrows between rotational stacks of Rydberg levels. Likewise, excitation into the ionization continuum of the $J^+ = 6$ stack at an energy of $49\,332\text{ cm}^{-1}$ can, at least in principle, lead to the inverse autoionization process described in the text, with the outgoing electron being captured and the underlying YO^+ ion being rotationally excited to the $J^+ = 8$ stack. In either case, these processes are only expected to occur when the total energy lies close to an ionization limit, where the density of Rydberg states becomes very large.

certainly cannot account for the intensity of the PFI-ZEKE features corresponding to odd values of $J'(A) - J^+ + 0.5$.

These observations suggest a channel-coupling mechanism, illustrated in Fig. 6, in which the (n, J^+) Rydberg level mixes with Rydberg levels having higher values of n and lower values of J^+ . Mixing between the (n, J^+) and $(n + \Delta n, J^+ - 1)$ levels provides a mechanism for pulsed field ionization of the high Rydberg states converging to $J^+ - 1$, even if high Rydberg states with $J^+ - 1$ carry no oscillator strength on their own. In addition, if Rydberg states converging to the J^+ rotational level are generally coupled to those converging to $J^+ - 1$, then Rydberg states converging to $J^+ - 1$ may be expected to couple to Rydberg states converging to $J^+ - 2$ as well, etc. A mechanism along these lines is necessary to explain the observation of all of the rotational states of YO^+ with $J^+ \leq J'(A) + 0.5$ in the PFI-ZEKE experiment, even though the dominant Rydberg progression only leads to production of $J^+ = J'(A) + 0.5$. Very likely, it is the strong dipolar field of the rotating YO^+ core that provides the requisite mechanism for the transfer of energy (and angular momentum) to the Rydberg electron. Such processes have been investigated in detail by Remacle and Levine, who have shown that the existence of a weak electric field is necessary for efficient channel coupling, through either a dipolar or quadrupolar coupling mechanism.⁴⁴ A similar suggestion has been made to account for the unexpectedly large range of rotational states observed in the pulsed field ionization of VO .⁵ In contrast, rotationally resolved PFI-ZEKE studies of the homonuclear diatomic, V_2^+ , found a more restricted range of rotational levels of the V_2^+ cation was produced, generally falling within the range expected for an $l=0$ Rydberg electron, $|J^+ - J'(A)| \leq 1.5$.¹ This observation reinforces the notion that the dipole moment of the underlying cation is essential for the coupling of Rydberg series corre-

sponding to different rotational channels. Rotational channel-coupling interactions similar to those proposed here have also been observed to occur in NO₂ (Ref. 45) and are reviewed by Merkt and Softley.⁴⁶ Vibrational channel-coupling interactions are observed to occur in the PFI-ZEKE spectra of Ag₂.^{47,48}

The coupling between Rydberg manifolds corresponding to different values of J^+ provides a means of decreasing J^+ from the value that carries the oscillator strength, with the loss in rotational energy made up by exciting the Rydberg electron to a higher Rydberg state. As judged from the spectra displayed in Fig. 5, these intermanifold couplings are remarkably efficient in coupling the initially populated J^+ value to all lower values. Indeed, there seems to be nothing preventing this coupling from continuing until a sufficiently low value of J^+ is reached so that the Rydberg electron is ejected into the ionization continuum, i.e., until rotational autoionization occurs. With this possibility in mind, it is surprising that any Rydberg states survive to be detected by pulsed field ionization at all.

It is now well-established that the PFI-ZEKE technique is successful because Rydberg states lying within approximately 8 cm⁻¹ of the ionization limit are strongly mixed by residual fields as small as 40 mV/cm.^{38,39} The dilution of the originally pumped, low l Rydberg state by l -mixing increases the lifetime of the Rydberg state by a factor of approximately n , and mixing of m_l states, particularly through collisions with ions, increases the lifetime of the Rydberg state by a second factor proportional to n . The long lifetimes of the "ZEKE states"³⁹ result because the Rydberg electron is usually in states of high l and m_l , where it rarely encounters the core. This phenomenon may explain the persistence of bound Rydberg states for a period of at least 3 μs despite the strong channel-coupling interactions which are present. For example, Rydberg states converging to $J^+=8$ of YO⁺, lying near 49 316 cm⁻¹ (which correspond to $n\sim 79$) are coupled to Rydberg states converging to $J^+=7$ ($n\sim 99$), these are coupled to Rydberg states converging to $J^+=6$ ($n\sim 141$), and these are finally coupled to the $J^+=5$ ($n\sim 446$) Rydberg states which readily undergo l - and m_l -mixing. These coupling matrix elements are dominated by the $\Delta J^+=0, \pm 1$, $\Delta l=0, \pm 1$ selection rules that derive from the dipolar coupling between the rotating YO⁺ core and the Rydberg electron. Assuming that the Rydberg series initially pumped corresponds to $l=0$, coupling of the originally pumped $J^+=8$ series to $J^+=5$ can change the orbital angular momentum to $l=3$. More importantly, however, the Rydberg electron now lies within the range of states for which l - and m_l -mixing can occur. Just when one more decrement of J^+ would lead to autoionization, the Rydberg electron can be spun off into states of high l and m_l where it seldom encounters the core, thereby greatly reducing the strength of the coupling to the ionization continuum.

If this idea is correct, it nicely explains the near-constancy of the peak intensities of the PFI-ZEKE spectra displayed in Fig. 5, at least for $J^+\leq J'(A)+0.5$. No matter which value of J^+ carries the oscillator strength, channel-coupling interactions quickly carry the molecule to states of lower J^+ until the range of l - and m_l -mixing is reached. At

that point, further channel-coupling interactions are minimized, and the molecules are stable, relative to rotational autoionization, until the pulsed field is applied. At that point in time they are field ionized, if they lie within the accessible range of an ionization threshold.

It is also observed in Fig. 5 that there are a number of weaker features in the spectra which correspond to $J^+ > J'(A)+0.5$. These are particularly evident in the spectrum recorded via excitation of $R_1(6)$, where values of J^+ as large as $J'(A)+4.5$ are observed. These high J^+ states require the Rydberg electron to have $l\geq 4$ for their observation. It seems highly unlikely that a Rydberg series with $l=4$ could carry sufficient intensity to account for these observations, so we are forced to consider alternative possibilities. An interesting alternative is an *inverse* rotational autoionization process, in which the probable $l=0$ Rydberg series that carries the oscillator strength allows the $J^+=J'(A)+0.5$ state to be prepared along with an outgoing electron that is truly unbound. Dipolar coupling between the rotating YO⁺ core and the outgoing electron can then increase both J^+ and l , allowing the outgoing electron to be recaptured into the bound high n, l states that form the long-lived ZEKE states.³⁹ Such a process could not be expected to be very efficient, explaining the small amplitude of the ZEKE signals for values of J^+ greater than $J'(A)+0.5$ in the spectra collected via excitation of $R_1(6)$ and $R_1(7)$.

An alternative to this possibility would be the capture of the outgoing electron by a *second* YO⁺ cation with the same value of J^+ as the YO⁺ cation that produced the electron. Again, dipolar coupling between the electron and the rotating ion is the interaction most likely to make this phenomenon possible. To fully distinguish between these possibilities, one would have to perform an isotopically substituted experiment, in which electrons originating from one isotopomer of YO might be captured by and subsequently field ionized from a different isotopomer. Such an experiment has not yet been performed. In a related experiment on C₆H₆ and C₆D₆, it was found that high Rydberg states of C₆H₆ could transfer the Rydberg electron to C₆D₆⁺ ions, to form high Rydberg states of the C₆D₆ molecule.^{39,49} In effect, this experiment on the isotopically substituted benzenes demonstrated the possibility of exchanging a weakly bound Rydberg electron from one ion to another. If two different YO⁺ ions are involved in the process responsible for the high-energy features in our spectra, however, the electron which is exchanged between them is unbound and channel-coupling interactions are still required to enable its attachment to the second cation. This makes the process envisioned here fundamentally different from that observed in the case of the isotopically substituted benzenes.

The weak features corresponding to $J^+ > J'(A)+0.5$ display linewidths in the range of 0.3 to 0.6 cm⁻¹, which are considerably narrower than the PFI-ZEKE peaks corresponding to $J^+\leq J'(A)+0.5$ and only slightly broader than the laser linewidth in this experiment (0.25 cm⁻¹). The observation of such narrow linewidths for the high-energy features implies that the inverse autoionization process can occur efficiently only if the electron kinetic energy falls within a narrow range corresponding to the highest values of n^* . The

strong dependence of the inverse autoionization process on electron kinetic energy (or the n^* value of the resulting bound Rydberg state) should come as no surprise, given that the density of Rydberg states grows proportionally to $n^{*5}/2R$. As the kinetic energy of the electron approaches the energy of an ionization threshold from below, the number of states that can be formed by electron attachment grows astronomically, making the attachment process far more likely to occur. This is true irrespective of whether the process is recapture of the outgoing electron by its own cation or transfer to a second YO^+ cation.

C. Energetics of YO and YO^+

As outlined in the Introduction, the ionization energy can be used to examine the bond strength of the molecule. For yttrium, the I.E. of the atom, measured spectroscopically from Rydberg series,⁵⁰ was determined to be $50\,144 \pm 1 \text{ cm}^{-1}$ or $6.2171 \pm 0.0001 \text{ eV}$ ($1 \text{ eV} = 8065.541 \text{ cm}^{-1}$). The I.E. of YO, as shown above, is $49\,304.316 \pm 0.031 \text{ cm}^{-1}$, or $6.112\,958 \pm 0.000\,004 \text{ eV}$. Thus, the I.E. of the atom is higher than that of the molecule by $0.1041 \pm 0.0001 \text{ eV}$, which is also the difference in bond dissociation energies, $D_0^0(\text{Y}^+-\text{O}) - D_0^0(\text{Y}-\text{O})$. This small difference is an indication that the bonding in the ion is similar to the bonding in the neutral. This is not surprising. The electron configurations in the $X^2\Sigma^+$ state of YO and in the $X^1\Sigma^+$ state of YO^+ are ... $11\sigma^2 5\pi^4 12\sigma^1$ and ... $11\sigma^2 5\pi^4$, respectively, in which the 12σ orbital is a nonbonding Y $5s/5p$ hybrid that is polarized away from the internuclear region. Therefore, the bonding character in YO and YO^+ is the same, hence, the very similar binding energy. The somewhat larger binding energy in the cation may be attributed to the charge-induced dipole interaction that is dominant at large separations between the Y^+ and O atoms. At smaller internuclear separations, an attractive Coulombic contribution to the potential energy is expected as Y^{2+}O^- character develops. This strongly attractive contribution is reduced in neutral YO, because of the smaller effective charge associated with the yttrium atom. Both the long-range ion-induced dipole interaction and the short-range Coulombic contribution lead to the expectation of a smaller bond length in YO^+ than in YO, and this is observed. Alternatively, the bond energy of neutral YO may be reduced as compared to that of YO^+ by the need to form a $5s/5p$ hybrid orbital in the neutral molecule. This requirement is absent in the ionic YO^+ , again leading to the expectation of a smaller bond length in YO^+ as compared to YO. The bond length in the $X^1\Sigma^+$ ($v=0$) state of YO^+ is $1.7463(6) \text{ \AA}$, whereas it is 1.7917 \AA in the $X^2\Sigma^+$ ($v=0$) state of YO.³⁷

As mentioned before, the bond strengths in YO and YO^+ have been determined experimentally. The best value for YO, taken from a critical evaluation of the available experimental data by Pedley and Marshall, is $7.41 \pm 0.12 \text{ eV}$.²⁶ For YO^+ , the measurements by Sievers *et al.* give $D_0^0(\text{Y}^+-\text{O}(g)) = 7.24 \pm 0.18 \text{ eV}$.²⁵ This yields $D_0^0(\text{Y}^+-\text{O}(g)) - D_0^0(\text{Y}-\text{O}(g)) = -0.17 \pm 0.22 \text{ eV}$, in contrast with the value of $0.1041 \pm 0.0001 \text{ eV}$ determined from accurate I.E. measurements. Either one or both of the disso-

ciation energy values are in error. In recent work on TiO, ZrO, NbO, and MoO, the reliability of the measurements of $D_0^0(\text{M}^+-\text{O})$ carried out using guided ion beam mass spectrometry was discussed and critically assessed.⁵¹ The assessment was that these measurements were accurate within their uncertainties. This assessment extends to $D_0^0(\text{Y}^+-\text{O})$. Consequently, from Eq. (1) we derive a value of $7.14 \pm 0.18 \text{ eV}$ for $D_0^0(\text{Y}-\text{O}(g))$. We believe that this new value is more reliable than the value quoted by Pedley and Marshall.²⁶ The new value is in excellent agreement with the value of $7.21 \pm 0.10 \text{ eV}$ measured by Rauh *et al.*, from a Knudsen effusate of YO in a mass spectrometer.²²

V. CONCLUSION

A spectroscopic study of the Rydberg states of YO accessed from particular rotational levels of the $A^2\Pi_{1/2}$, $v=0$ state has been combined with a pulsed field ionization, zero electron kinetic energy (PFI-ZEKE) investigation. The results provide accurate values of the ionization energy of YO, I.E.(YO) = $49\,304.316(31) \text{ cm}^{-1}$ [$6.112\,958(4) \text{ eV}$], and of the rotational constant (and bond length) of the YO^+ cation in its $X^1\Sigma^+$, $v=0$ ground state, $B_0^+ = 0.4078(3) \text{ cm}^{-1}$ [$r_0 = 1.7463(6) \text{ \AA}$]. This study reduces the uncertainty in the ionization energy of YO, as known from previous experiments, by a factor of over 10^4 , while also providing the first measurement of the bond length of the YO cation. The improved value of I.E.(YO) combined with the known ionization energy of atomic yttrium then leads to the result $D_0^0(\text{Y}^+-\text{O}) - D_0^0(\text{Y}-\text{O}) = 0.1041 \pm 0.0001 \text{ eV}$. Using the value of $D_0^0(\text{Y}^+-\text{O})$ obtained in guided ion beam collision-induced dissociation measurements, $D_0^0(\text{Y}^+-\text{O}) = 7.24 \pm 0.18 \text{ eV}$, an improved value of $D_0^0(\text{Y}-\text{O}) = 7.14 \pm 0.18 \text{ eV}$ is obtained. This represents a correction of -0.27 eV to the previously accepted value.

The Rydberg spectra observed display strong lines corresponding to $J^+ = J'(A) + 0.5$, along with weaker ones corresponding to $J^+ = J'(A) - 1.5$, where $J'(A)$ specifies the rotational level of the $A^2\Pi_{1/2}$ state. This is consistent with a Hund's case (*d*) coupling scheme in which the Rydberg electron has an orbital angular momentum, l , of 0 or 2. In contrast, the PFI-ZEKE spectra display strong transitions to all values of $J^+ \leq J'(A) + 0.5$. This unexpected result is interpreted in terms of a channel-coupling interaction in which the dipole moment of the rotating YO^+ molecule can induce changes in l and J^+ subject to the dipolar coupling matrix element selection rule, $\Delta J^+ = \pm 1$, $\Delta l = \pm 1$. Through this mechanism, J^+ can be sequentially reduced while the principal quantum numbers n^* and l are increased, until the value of n^* becomes so large that l - and m_l -mixing occurs due to the small residual fields and ion densities present in the instrument. At that point, the states become both very long-lived and ionizable by a subsequent pulsed field as weak as 0.3 V/cm . The channel-coupling mechanism also appears to induce an inverse autoionization process in which an unbound electron with a low value of l is captured either by its low- $J^+\text{YO}^+$ cation or by a second YO^+ cation with the same value of J^+ . This inverse autoionization process is extremely sensitive to the electron kinetic energy, leading to

narrow peaks in the PFI-ZEKE spectrum which are only slightly broader than the laser linewidth employed for this study (0.25 cm^{-1}).

ACKNOWLEDGMENTS

M.D.M. and P.B.A. thank the National Science Foundation for support of this research under Grant Number CHE-9626557 and CHE-9877162, and M.D.M. also acknowledges the donors of the Petroleum Research Fund, administered by the American Chemical Society, for partial support of this work. C.L. acknowledges support from the Natural Sciences and Engineering Research Council (NSERC) of Canada. The authors are grateful to Dr. Jim Watson for calculating the line strengths for rotational branches, helpful comments and discussion, and for reading the final draft of the manuscript. Issued as NRCC# 40900.

- ¹D. S. Yang, A. M. James, D. M. Rayner, and P. A. Hackett, *J. Chem. Phys.* **102**, 3129 (1995).
- ²R. L. Asher, D. Bellert, T. Buthelezi, and P. J. Brucat, *Chem. Phys. Lett.* **224**, 525 (1994).
- ³D. Bellert, T. Buthelezi, V. Lewis, K. Dezfulian, D. Reed, T. Hayes, and P. J. Brucat, *Chem. Phys. Lett.* **256**, 555 (1996).
- ⁴A. J. Merer, A. S.-C. Cheung, and A. W. Taylor, *J. Mol. Spectrosc.* **108**, 343 (1984).
- ⁵J. Harrington and J. C. Weisshaar, *J. Chem. Phys.* **97**, 2809 (1992).
- ⁶J. G. Phillips and S. P. Davis, *Astrophys. J.* **234**, 393 (1979).
- ⁷W. J. Balfour and B. Lindgren, *Phys. Scr.* **22**, 36 (1980).
- ⁸C. J. Cheetham and R. F. Barrow, *Trans. Faraday Soc.* **63**, 1835 (1976).
- ⁹C. Fosca, B. Pinchemel, D. Collet, and T. R. Huet, *J. Mol. Spectrosc.* **189**, 254 (1998).
- ¹⁰W. J. Balfour and K. S. Chandrasekhar, *J. Mol. Spectrosc.* **139**, 245 (1990).
- ¹¹C. Fosca, C. Dufour, B. Pinchemel, I. H. Bachir, and T. R. Huet, *J. Chem. Phys.* **106**, 9044 (1997).
- ¹²L. A. Kaledin and M. C. Heaven, *J. Chem. Phys.* **107**, 7020 (1997).
- ¹³C. Fosca, B. Pinchemel, J. L. Femenias, and T. R. Huet, *J. Chem. Phys.* **107**, 10365 (1997).
- ¹⁴L. A. Kaledin and M. C. Heaven, *J. Mol. Spectrosc.* **184**, 113 (1997).
- ¹⁵E. A. Shenyavskaya and B. S. Ryabov, *J. Mol. Spectrosc.* **63**, 23 (1976).
- ¹⁶E. A. Shenyavskaya and L. V. Gurvich, *J. Mol. Spectrosc.* **81**, 152 (1980).
- ¹⁷L. A. Kaledin, A. L. Kaledin, and M. C. Heaven, *J. Mol. Spectrosc.* **179**, 246 (1996).
- ¹⁸T. Hayes, D. Bellert, T. Buthelezi, and P. J. Brucat, *Chem. Phys. Lett.* **287**, 22 (1998).
- ¹⁹R. L. Asher, D. Bellert, T. Buthelezi, and P. J. Brucat, *Chem. Phys. Lett.* **227**, 277 (1994).
- ²⁰T. Buthelezi, D. Bellert, V. Lewis, and P. J. Brucat, *Chem. Phys. Lett.* **242**, 627 (1995).
- ²¹R. L. Asher, D. Bellert, T. Buthelezi, D. Lessen, and P. J. Brucat, *Chem. Phys. Lett.* **234**, 119 (1995).
- ²²E. G. Rauh and R. J. Ackermann, *J. Chem. Phys.* **60**, 1396 (1974).
- ²³M. B. Liu and P. G. Wahlbeck, *High. Temp. Sci.* **6**, 179 (1974).
- ²⁴E. Murad and D. L. Hildenbrand, *J. Chem. Phys.* **73**, 4005 (1980).
- ²⁵M. R. Sievers, Y.-M. Chen, and P. B. Armentrout, *J. Chem. Phys.* **105**, 6322 (1996).
- ²⁶J. B. Pedley and E. M. Marshall, *J. Phys. Chem. Ref. Data* **12**, 967 (1983).
- ²⁷A. M. James, P. Kowalczyk, E. Langlois, M. D. Campbell, A. Ogawa, and B. Simard, *J. Chem. Phys.* **101**, 4485 (1994).
- ²⁸D. Proch and T. Trickl, *Rev. Sci. Instrum.* **60**, 713 (1989).
- ²⁹W. C. Wiley and I. H. McLaren, *Rev. Sci. Instrum.* **26**, 1150 (1955).
- ³⁰J. B. Hopkins, P. R. R. Langridge-Smith, M. D. Morse, and R. E. Smalley, *J. Chem. Phys.* **78**, 1627 (1983).
- ³¹R. J. Noll, L. L. Ochalla, and J. C. Weisshaar, *Rev. Sci. Instrum.* **62**, 246 (1991).
- ³²G. Beck, *Rev. Sci. Instrum.* **47**, 849 (1979).
- ³³J. L. Wiza, *Nucl. Instrum. Methods* **162**, 587 (1979).
- ³⁴H. M. Crosswhite, Fe-Ne *Hollow Cathode Tables* (Johns Hopkins University Press, Baltimore, 1965).
- ³⁵S. Gerstenkorn and P. Luc, *Atlas du Spectre d'Absorption de la Molecule d'Iode entre 14 800-20 000 cm⁻¹* (CNRS, Paris, 1978).
- ³⁶S. Gerstenkorn and P. Luc, *Rev. Phys. Appl.* **14**, 791 (1979).
- ³⁷A. Bernard, R. Bacis, and P. Luc, *Astrophys. J.* **227**, 338 (1979).
- ³⁸W. A. Chupka, *J. Chem. Phys.* **98**, 4520 (1993).
- ³⁹E. W. Schlag, *ZEKE Spectroscopy* (Cambridge University Press, Cambridge, 1998).
- ⁴⁰J. K. G. Watson, *J. Chem. Phys.* **108**, 820 (1998).
- ⁴¹J. Xie and R. N. Zare, *J. Chem. Phys.* **93**, 3033 (1990).
- ⁴²J. W. C. Johns, in *A Specialist Periodical Report*, Vol. 2 (The Chemical Society of London, London, 1974), pp. 513.
- ⁴³J. K. G. Watson (personal communication).
- ⁴⁴F. Remacle and R. D. Levine, *J. Chem. Phys.* **105**, 4649 (1996).
- ⁴⁵G. P. Bryant, Y. Jiang, M. Martin, and E. R. Grant, *J. Phys. Chem.* **96**, 6875 (1992).
- ⁴⁶F. Merkt and T. P. Softley, *Int. Rev. Phys. Chem.* **12**, 205 (1993).
- ⁴⁷G. I. Nemeth, H. Ungar, C. Yeretizian, H. L. Selzle, and E. W. Schlag, *Chem. Phys. Lett.* **228**, 1 (1994).
- ⁴⁸C. Yeretizian, R. H. Hermann, H. Ungar, H. L. Selzle, E. W. Schlag, and S. H. Lin, *Chem. Phys. Lett.* **239**, 61 (1995).
- ⁴⁹C. Alt, W. G. Scherzer, H. L. Selzle, and E. W. Schlag, *Chem. Phys. Lett.* **224**, 366 (1994).
- ⁵⁰W. R. S. Garton, E. M. Reeves, F. S. Tomkins, and B. Ercoli, *Proc. R. Soc. London, Ser. A* **333**, 17 (1973).
- ⁵¹H.-P. Looock, B. Simard, S. Wallin, and C. Linton, *J. Chem. Phys.* **109**, 8980 (1998).